

FLOW STRUCTURE IN THE BASE REGION OF RE-ENTRY VEHICLE WITH SUPERSONIC BRAKING PLUMES IMPINGING WITH LANDING SURFACE

A.A. Dyadkin¹, V.P. Sukhorukov¹, G.A. Trashkov¹, V.F. Volkov², V.I. Zapryagaev², N.P. Kiselev²

1 Korolev Energiya Rocket and Space Corporation, 141070 Korolev, Moskovskaya Oblast, Russia,

2 Khristianovich Institute of Theoretical and Applied Mechanics SB RAS, 630090 Novosibirsk, Russia

zapr@itam.nsc.ru

Keywords: *re-entry vehicle, landing surface, supersonic plumes, flow structure*

Abstract

Results of an experimental study of the aerodynamic characteristics and flow structure in the vicinity of a re-entry vehicle (RV) with supersonic braking plumes impinging onto landing surface (LS) are reported. The experiments were carried out for two small-scale (1:15) RV models provided with pressure taps, with cold air being used as the test gas. The RV models differed from one another both in the number of braking plumes (16 and 8) and in the geometric arrangement of nozzles on the RV body. The influence of LS-reflected jets on the distribution of pressure over the RV surface was examined. Experimental data demonstrating effects due to the angle of inclination of the RV axis to the LS plane and due to the RV-to-LS distance are reported. Visualization of the flow structure due to supersonic braking plumes and visualization of limit streamlines on landing surface are presented. A brief description of designs of the used models, and also of the employed experimental equipment and procedure, is given. Numerical simulated data for the flow structure arising during the interaction of RV plumes with the landing surface are outlined.

1. Introduction

Studies aimed at the development of future re-entry vehicles using multi-plume braking

systems for deceleration of RV in the vicinity of landing surface are currently under way. The flow structure in the vicinity of such vehicles, and aerodynamic characteristics of the vehicles during supersonic plume interaction with supersonic flow at deceleration were reported in [1]. Not less difficult is the problem on studying the flow structure in the vicinity of a re-entry vehicle approaching a landing surface. For such a braking method, an efficient control of the multi-plume braking system at landing regimes needs to be ensured. It is required to evaluate the gas-dynamic and acoustic loads that will act on the RV body during landing. As the non-isobaric supersonic jets produced by the multi-plume braking system interact with the landing surface, secondary flows form in the region between the RV body and the landing surface. Also, secondary gas streams due to the interaction of the plumes with the surface may arise. During the interaction of a multi-plume system with the landing surface, complex vortex flows arise in the region between the RV frontal panel (front heat shield) and the landing surface; the formation of such flows induces additional gas-dynamic forces and force moments that act on the RV body [2]. Investigation into the structure of the vortex flow and into the flow pulsation characteristics in the separation region formed as the supersonic jet streams interact with the landing surface therefore presents a vital problem.

2. Experimental facility

The jet facility (JF) ITAM SB RAS intend for experimental investigation of gasdynamic flow structure as free supersonic jet flows as impinging with obstacle jets. The jet facility (JF) used in the present study has a prechamber installed in upright position. At the center of the upper flange of the chamber, a connector assembly for connecting different nozzles was provided. The chamber was shaped as a cylinder with inner diameter 330 mm; it contained a honeycomb at the inlet and a deturbulizing grid for flattening the air stream at the outlet. The entrance to the channel through which the air from the settling chamber was supplied to the nozzle was made as a lemniscate-shaped path. The jet facility was connected to a high-pressure air supply system (pressure up to 200 bar) with an air pipeline whose effective diameter was 130 mm; the pipeline ensured a sufficiently high mass flow rate of air (up to 20 kg/s), and it was provided with a special valve for control a predetermined value pressure in the prechamber. Runs of the experimental facility were initiated and the required gas-dynamic regimes, maintained, using a remote console. A photo of the jet facility is shown in Fig. 1. In the photo, an RV model and the landing surface, a support beam, a tilting mechanism, and a Tepler optic device are seen. The prechamber and the walls of the experimental facility were covered with an acoustic foam rubber layer. The possibility of variation of the angle between the longitudinal axis of RV and the local vertical to the landing surface φ was implemented.

A data acquisition system was developed to enable, in automatic mode, the collection of the values of gasdynamic flow parameters of experiments and JF geometric parameters. A diagram of the system is shown in Fig. 2.

The data acquisition system comprised a personal computer, a high-precision Agilent multimeter (model HP 3490A) equipped with a multiplexer, and an I-7019 analog-to-digital converter (ADC). For measuring the gasdynamic parameters of the facility, OWEN pressure sensors with measurement range 1 bar (ambient pressure p_h) and 160 bar (prechamber pressure P_0) were used.



Fig. 1. Photo of the experimental facility.

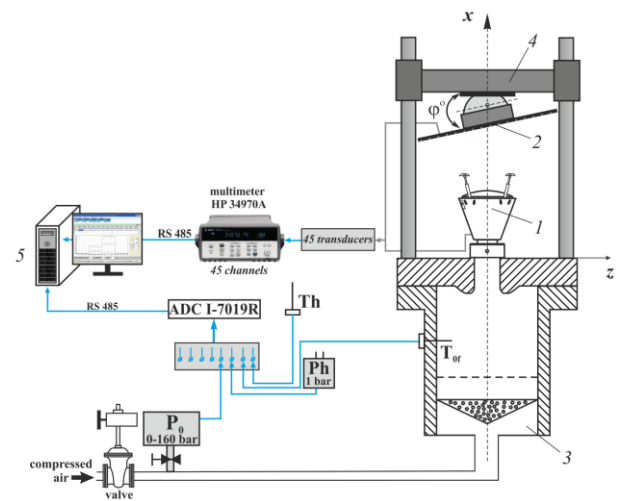


Fig. 2. Experimental arrangement:
 1 – reentry vehicle (RV); 2- landing surface (LS); 3 – compression chamber; 4 – support beam; 5 - PC.

Measurements of temperature were conducted with the help of Honeywell resistance temperature sensors that were located in the compression chamber and in the room in which the experimental jet facility was installed. The pressure p_h was measured immediately in the room at a distance of four meters from nozzle exit plane. The time interval between the readings was 0.4 s.

The analog signals from pressure sensors that measured the pressures acting on the RV body and on the landing surface were transferred, through the HP multimeter, to a digital voltmeter to be digitized and then fed into PC memory (Fig. 2). The parameters of the

experimental facility were transferred through an I-7019R ADC card. The signals from the sensors were recalculated into the values of physical quantities (pressure, temperature).

Measurements of the static pressures at tap locations were carried out using high-precision TDM absolute-pressure sensors.

The experimental procedure was as follows. Before to each run of the jet facility and after its run without air supply, measurements were performed. In data processing, the mean values of the pressures that were measured prior to and after the run were subtracted from the values of pressures measured during the run. After establishment of a preset gas-dynamic regime, which was monitored by indications of a manometer and the pressure sensor that measured the pressure P_0 in the prechamber, measurements of pressures on the RV and LS models were carried out.

A diagram illustrating the variation of measured pressures in a single run of the jet facility is shown in Fig. 3.

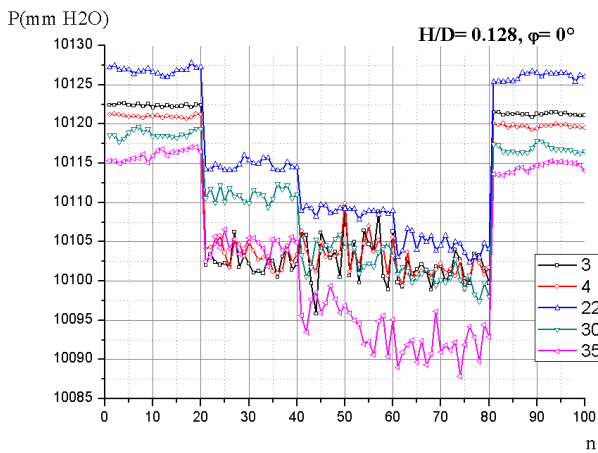


Fig. 3. Typical variation of measured pressure values during a single run of the experimental facility (measurement of pressures on the surface of RV body), 3, 4, 22, 30, and 35 – numbers of the points on the RV surface.

The pressure values for $n = 0-20$ and $81-100$ refer to pressure measurements performed without air supply; in processing experimental data, those values were to be subtracted from the pressure values measured in facility runs with air supply. A total of 20 measurements at

$N_{pr} = P_0/p_h = 60$ ($n = 21-40$), $N_{pr} = 90$ ($n = 41-60$), and $N_{pr} = 120$ ($n = 61-80$) were made. It should be noted here that, in each measurement, averaging over ten readings was performed. The total measurement time per one reading was 2.5 s. In the figure, pressure fluctuations due to stream pulsations are seen.

Visualization of the flow pattern in the region between the RV and LS surfaces was performed with the help of a schlieren device IAB-451 and a digital CCD camera with resolution 1400×1000 pixels and exposure time $125 \mu s$. The diameter of the optical glasses of the IAB-451 schlieren instrument was 230 mm. Visualization of flow streamlines on the surface of RV model and on the model of LS was performed using soot-oil coatings.

The experimental procedure comprised a study of the gasdynamic pattern of the flow in region between the re-entry vehicle and the landing surface. Data on the distribution of pressure on the RV and LS surfaces as dependent on the RV-to-LS distance ($H/D = 0.4, 1.0, \text{ and } 1.4$; D is the midsection diameter, $D = 293$ mm) and on the angle between the longitudinal axis of RV and the local vertical ϕ at various jet discharge regimes were obtained. From measured values of the pressure on the RV surface, the integral forces and the integral force moments acting on the RV body were calculated.

3. Results of the experimental study

In the present publication, we report on the results of an experimental study and numerical simulations performed for two RV models with different arrangements and different quantity of braking plumes nozzles.

3.1. M-16 model

The RV model with 16 nozzles located on the RV frontal panel is shown in Fig. 4. The model nozzles have identical geometric dimensions, and they were grouped in four nozzle assemblies located at angular spacing 90 degrees around the circumference of the RV frontal panel. The geometric Mach number of model nozzles was equal to the Mach number of full-scale nozzles, $M_a = 3.32$, and the diameter of

model nozzles at nozzle exits was $D_a = 6.0$ mm. The supersonic part of each nozzle was shaped as a cone with expansion angle 24 degrees. Tests were performed both for the design jet discharge regime with $N_{pr} = P_0/p_h = 58.9$ and for the half-thrust regime with $N_{pr} = 29.5$.



Fig. 4. The RV model with 16 nozzles on the RV frontal panel.

Typical distribution of normalized excess pressure over the surface of RV frontal panel for three angles of inclination of the RV axis to LS, $\varphi = 0, 4,$ and 10 degrees are shown in Fig. 5. The excess pressure was calculated as $\Delta P = p_i - p_h$, where p_i is the measured absolute pressure, p_h is ambient pressure.

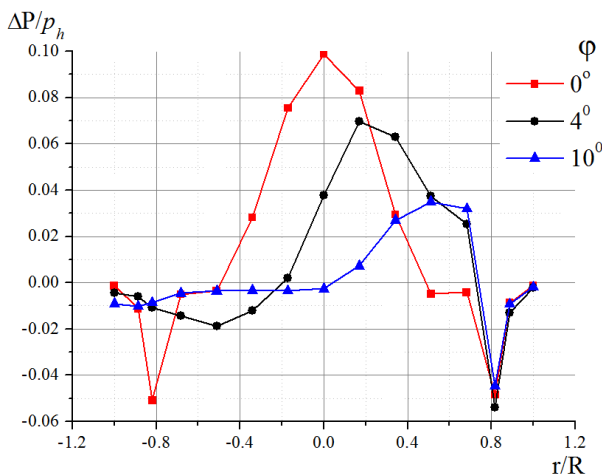


Fig. 5. Distribution of pressure on the surface of RV frontal panel for various angles φ at $N_{pr} = 58.9$ and $H/D = 0.4$.

Data are shown for the separation between the apex of RV frontal panel and LS $H/D = 0.4$; the pressure taps were located over the radius r in the plane of LS inclination angle. For normal orientation of the surface ($\varphi = 0$), the distribution of normalized excess pressure is symmetric about the axis of RV body. On increasing the angle of obstacle inclination, the registered pressure maximum decreases in value, and its position gets shifted; this case refers to variation of the intensity of reverse flows in the region between the frontal panel and LS. The reduced pressure registered at $r/R = 0.8$ refers to pressure taps that were located in the vicinity of nozzle exits. The pressure on the conic lateral surface differs insignificantly from the pressure in the ambient space p_h , which is equal to atmospheric pressure.

When the RV-to-LS distance is increased over $H/D = 1.0$, the pressure on the RV surface remains differing little from the ambient pressure. The latter fact is illustrated by Fig. 6, which shows the distribution of normalized excess pressure over the surface of RV frontal panel for three values of H/D and for $\varphi = 4^\circ$.

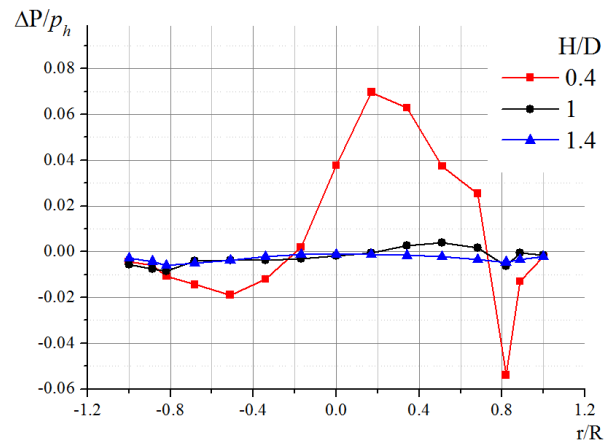


Fig. 6. Distribution of pressure on the surface of RV for various values of H/D at $N_{pr} = 58.9$ and $\varphi = 4^\circ$.

The distribution of normalized excess pressure over LS for the angle of obstacle inclination $\varphi = 4^\circ$ and for RV-to-LS distance $H/D = 0.4, 1.0,$ and 1.4 is shown in Fig. 7. The data are shown in the diametric plane passing through the RV axis in the plane of obstacle

inclination. Some asymmetry in the distribution of pressure due to the inclination of the obstacle, and also a decrease of the maximal registered normalized excess pressure from 1.1 to 0.15 that occurs on increasing the relative RV-to-LS distance from $H/D=0.4$ to 1.4, are observed. The latter decrease is both due to the decrease of the maximal dynamic pressure in the supersonic jet that occurs with increasing the distance from nozzle exits and due to the change of the regime of interaction of supersonic jets with the surface that occurs on increasing the angle φ . The maximal excess pressures on LS registered for the nominal jet discharge regime at the minimal distance $H/D=0.128$, amount to 120 kPa.

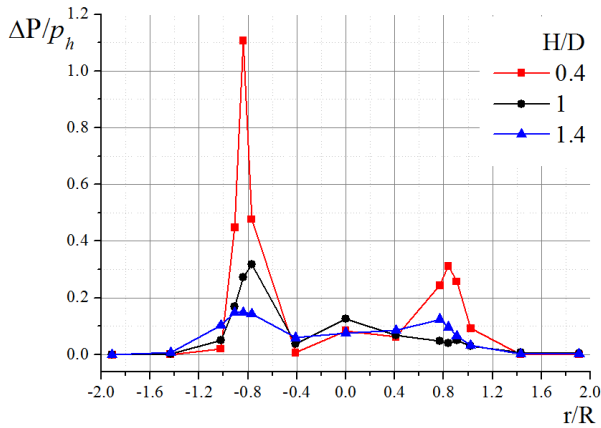


Fig. 7. Distribution of pressure over LS for various values of H/D in the case of $N_{pr}=58.9$ and $\varphi=4^\circ$.

Schlieren visualization of the flow in the region between the frontal panel of RV and the landing surface is shown in Fig. 8 for normal orientation of the obstacle ($\varphi=0$), design jet discharge regime ($N_{pr}=58.9$), and $H/D=0.4$. The shock-wave structure of the flow over the initial length of the jets, and also the turbulent flow structure that arises during the interaction of jets with the obstacle, are distinctly observed. Since the optical axis of the Tepler device did not coincide with the RV axis, the images contain, instead of one, two closely spaced jets exhausted from different four-nozzle assemblies. The latter explains some smearing of the shock-wave structures over the initial length of supersonic jets.

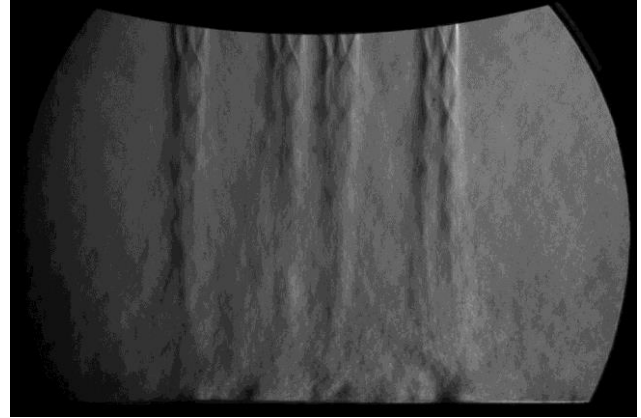


Fig. 8. Schlieren photo of a flow structure in region between RV and LS for $H/D=0.4$, $N_{pr}=58.9$ and $\varphi=0^\circ$.

Visualization of limiting flow streamlines on LS was performed with the help of a soot-oil coating for two representative jet discharge regimes with $H/D=1.0$ and $\varphi=0^\circ$ and 10° . The stream spreading patterns shown in Figs. 9 and 10 point to the occurrence of essentially different flow patterns on the landing surface in the cases of $\varphi=0^\circ$ and 10° . Evidently, at normal interaction each jet group comprising four jets produced by the retro-rocket system forms a flow one part of which is directed outwards while the other part is directed inwards. On the landing surface, the four converging stream interact with each other at the center of the obstacle to form an intensive ascending flow. The latter leads to an increase of pressure in the central region of RV frontal panel (see Figs. 5 and 6).

On tilting the obstacle, the flow pattern shows a change, the flow asymmetry in the vicinity of LS being observed at angles $\varphi=4^\circ$ and 10° . A through-flow near LS is formed and the rate of the reverse flows is decreased. Here, the soot-oil visualization picture of the flow on the LS surface is similar to the flow pattern formed by an annular nozzle structure with densely packed of jet nozzles [2].

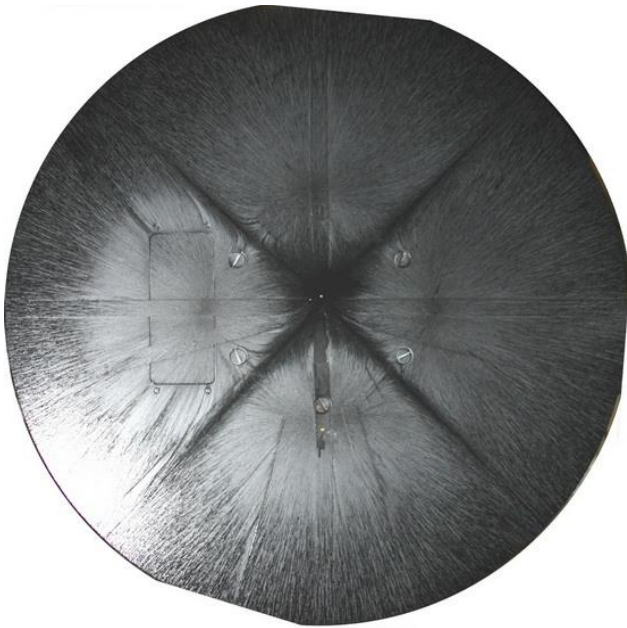


Fig. 9. Soot-oil visualization of the flow on the landing surface for $H/D= 1.0$, $N_{pr}= 58.9$ and $\varphi= 0^\circ$.

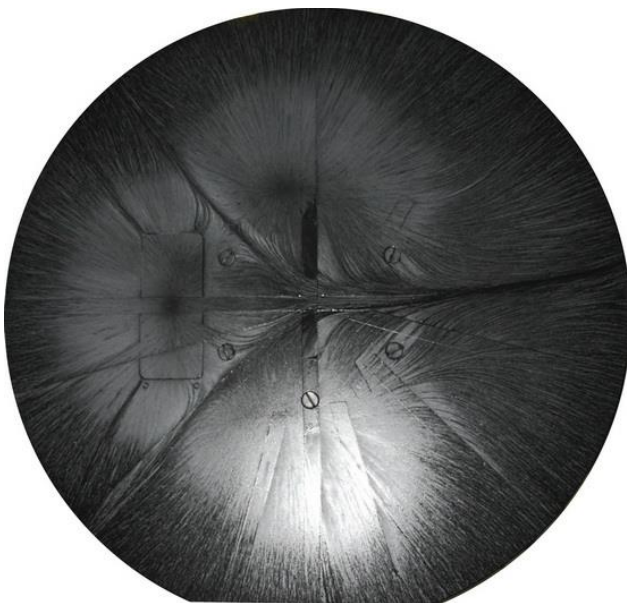


Fig. 10. Soot-oil visualization of the flow on the landing surface in the case of $H/D= 1.0$, $N_{pr}= 58.9$ and $\varphi= 10^\circ$

3.2 M-8 model

With goal of minimization of the action on RV body due to the secondary streams formed as a result of the interaction of supersonic jets with LS, and also for minimization of the gas-dynamic forces and force moments acting on the

re-entry vehicle at landing, we have made a modification of the configuration of RV.

Another configuration of RV construction with brake plumes nozzles located on the conic lateral surface was proposed.

A photo of the RV model with eight brake plumes nozzles are located on the lateral surface and four nozzle also are located on the lateral surface for damping the horizontal velocity is shown in Fig. 11.



Fig. 11. Photo of the RV model

For M-8 model, all nozzles have identical geometric dimensions. The axes of the retro-rocket nozzles for damping the vertical velocity were located in planes that were parallel to the stabilization planes I-III and II-IV of RV; those planes were inclined to the longitudinal axis of RV at an angle of 45 degrees. The M-8 model was also provided with a nozzle assembly intended for control of RV horizontal velocity; this assembly comprised four nozzles also located on the lateral surface (Fig. 12). The geometric Mach number of model nozzles was equal to the Mach number of full-scale nozzles, $M_a= 3.5$, and the diameter of model nozzles at nozzle exits was $D_a= 6.5$ mm. The supersonic part of each nozzle was shaped as a cone with expansive angle 34 degrees. The design regime of the nozzle flows refers to the conditions with

$N_{pr}=P_0/p_h=76.3$. Experiments were carried out for $N_{pr}= 60, 90,$ and 120 . The RV-to-LS distance was $H/D= 0.128, 0.4, 1.0,$ or 1.4 . The angle of inclination of the obstacle surface to the RV normal was $\varphi=0, -4,$ or -12 degrees.

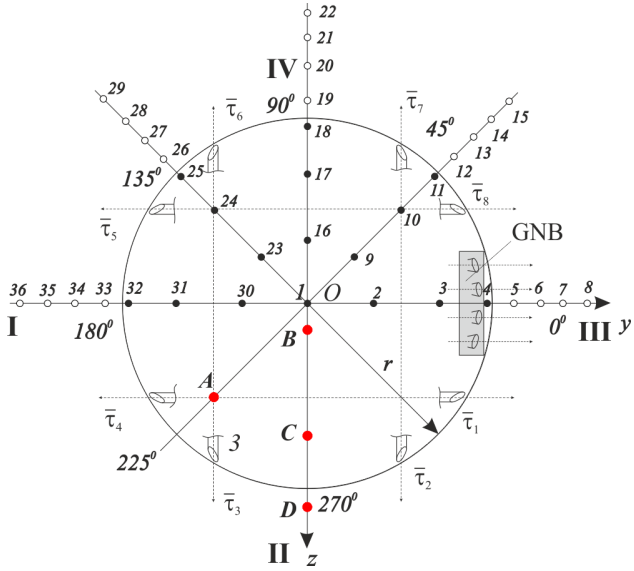


Fig. 12. The arrangement of braking nozzles ($\tau_1 - \tau_8$) and a four-nozzle assembly for correcting the horizontal drift of RV. The locations of the points at which the pressures on the RV surface were measured are denoted with the numerals 1-36. The locations of pressure pulsation sensors are denoted with the letters A, B, C, and D.

The decrease in the number of braking jets and the existence of a jet inclination angle has led to a substantial weakening of reflected flows near LS. This observation is supported experimental data, lower pressure values was reiterated on the frontal panel even at small RV-to-LS distances. A typical distribution of pressure over the surface of RV frontal panel is shown in Fig. 13. The pressure is seen to be somewhat lower than atmospheric pressure ($\Delta P/p_h \sim -0.001$). The local increase of pressure on the frontal surface ($\Delta P/p_h = 0.004$) and the fall of pressure on the conical lateral surface of RV ($\Delta P/p_h = -0.007$) were due to the aerodynamic interference of the high-pressure supersonic jets with the RV surface.

Activation of the jet assembly intended for damping the horizontal velocity (Fig. 12) no substantial influence on the distribution of pressure over the RV surface.

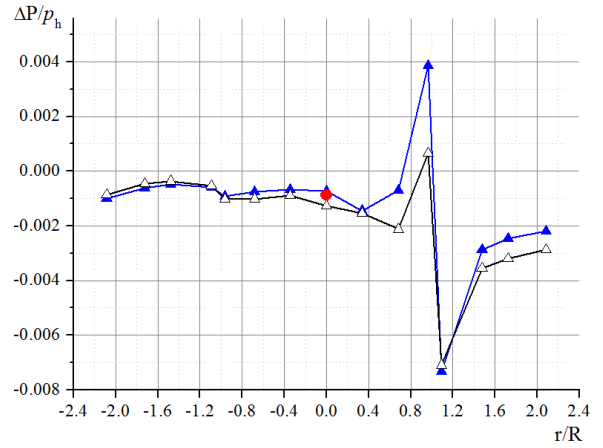


Fig. 13. Distribution of normalized excess pressure over the surface of RV frontal panel in the plane of symmetry I-III of the RV model (only vertical jets) for $H/D= 0.128, \varphi= -12^\circ,$ and $N_{pr} = 120$.

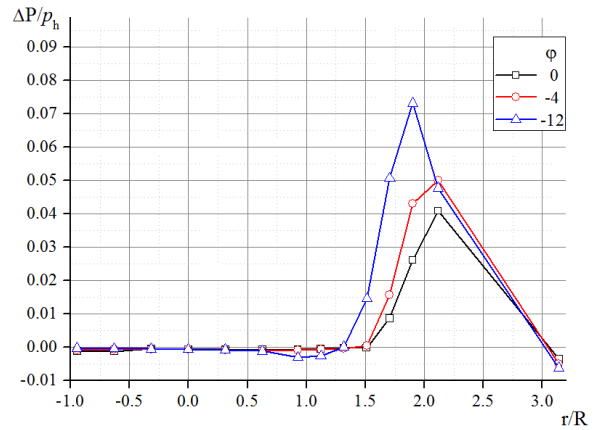


Fig. 14. Distribution of normalized excess pressure over the model of LS in the plane of symmetry of RV at various angles φ for $H/D=0.256$ and $N_{pr}= 120$.

Typical values of the normalized excess pressure acting on LS at various angles of obstacle inclination, $\varphi= 0, -4.0,$ and -12 degrees, and at $H/D=0.256$ are shown in Fig. 14. A decrease of the maximal pressure with increasing the angle of obstacle inclination is evident; this decrease is both due to the increase of the distance from the point of interaction of the jets with LS and due to the modification of the flow structure in the region of the interaction which occurs during the change of the angle of obstacle inclination.

A schlieren photo illustrating the gas-dynamic structure of supersonic braking jets

emanating out of nozzles at $N_{pr}=90$ is shown in Fig. 15. Some smearing of the initial length of the jets is due to the fact that the shown image presents a superposition of two jets (τ_1 and τ_8 , see Fig. 12). It is seen that the increase of jet diameter with distance from nozzle exit is insignificant, with the angle of inclination of the jets to the RV axis being in compliance with the orientation of nozzle axes (45 degrees).

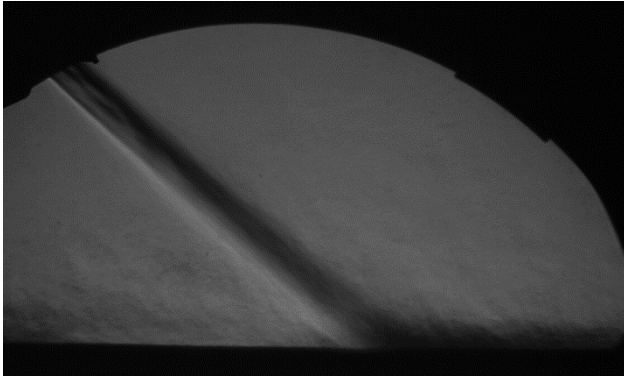


Fig. 15. Schlieren visualization of the jet flow for $M_a=3.5$, $N_{pr}=90$, $H/D=0.128$, and $\varphi=0^\circ$ (exposure time 0.4 ms).

4. Simulated data

We have performed a numerical study of the flow structure and the distribution of pressure on the RV and LS surfaces for the RV configuration with nozzles located on the lateral surface of RV body for RV hovering heights $H/D = 0.125 - 0.513$ with allowance for the operation of the soft-landing rocket system and for the interaction of RV plumes with landing surface at $N_{pr}=120$.

The computation domain was the space bounded by the RV surface (inner surface), by an outer boundary, and by the landing surface (see Fig. 16). The same figure shows the finite-difference mesh in the nozzle assembly of the propulsion system and in the space between RV and LS. The represented mesh space comprises 4.4 million nodal points.

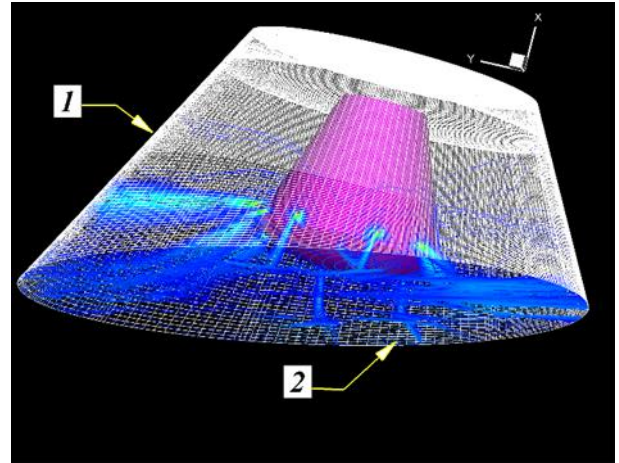


Fig. 16. Computation domain: 1 – outer boundary, 2 – landing surface.

We consider the hovering of the re-entry vehicle over the earth surface with operating retro-rocket engines for damping the vertical and horizontal velocities of RV.

For the regime of RV hovering at a height $H/D=0.128$ above the landing surface and at the inclination angle $\varphi=0^\circ$, Figs. 17 - 19 demonstrate the main specific features of the flow structure in the vicinity of RV and the distributions of local pressures on the RV frontal panel and on the landing surface as revealed in numerical simulations.

Flow streamlines and, in particular, the tracks of flow streamlines on the RV surface in the plane of symmetry of RV are shown in Fig. 17.

The tracks of flow streamlines in Fig. 17 point to the fact that, in the space between the jets a vortex flow with local counter-flows directed, in the vicinity of LS, towards the center of landing area, forms. The interaction between the counter-flows leads to the formation of an ascending flow moving towards the center of the RV frontal panel.

Contour lines of the excess pressure on the surface of RV frontal panel are shown in Fig. 18; values of the pressure at several points are indicated. The color gradation in the figure refers to excess-pressure values indicated in the scale (kPa).

FLOW STRUCTURE IN THE BASE REGION OF RE-ENTRY VEHICLE WITH BRAKING SUPERSONIC PLUMES IMPINGING WITH LANDING SURFACE

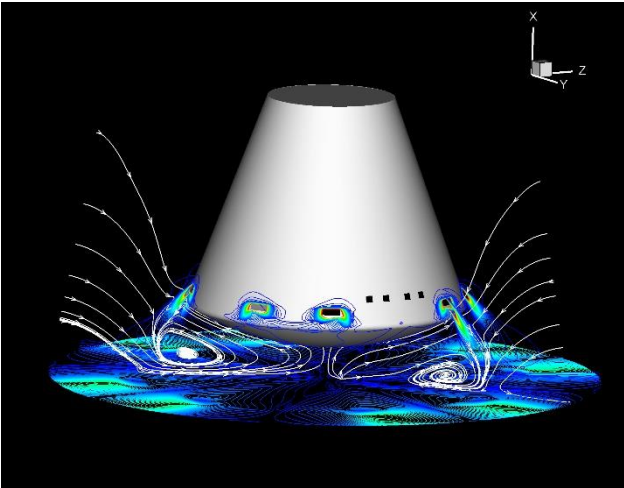


Fig. 17. Flow structure in the region between RV and LS in the case of $\varphi=0^\circ$ and $H/D= 0.128$.

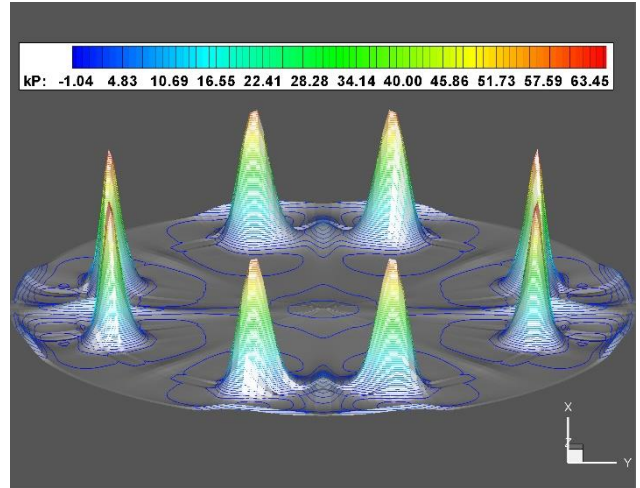


Fig.19. Distribution of pressure on the landing surface in the case of $H/D=0.128$ and $\varphi =0^\circ$.

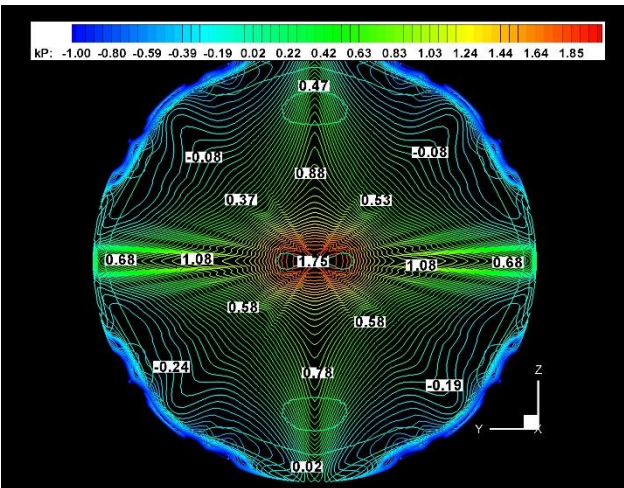


Fig. 18. Distribution of pressure on the frontal panel of RV model.

In the figure, two mutually perpendicular directions along which elevated pressure values are realized can be identified. The occurrence of such directions can be explained with the orientation of RV vertical braking nozzles. At the center of the frontal panel, a pressure maximum due to the reverse flow from LS is registered. The rise of the pressure in the planes $z=0$ and $y=0$ is due to the spreading of the flow from the center of the frontal panel towards the periphery (Fig. 18).

The interaction between the jet flows produced by braking plumes and the landing surface is illustrated by Fig. 19. In the figure, eight excess-pressure maxima ($\Delta P \sim 70$ kPa) due to the interaction of RV braking plumes with LS are clearly seen. As the jets spread over the landing surface, an interaction between secondary streams is registered. This interaction induces a slight rise of pressure in between the pressure maxima due to the impingement of braking jets onto LS.

Conclusions

An experimental study of the flow structure and the distribution of the mean pressure over the surface of re-entry vehicle (RV) and landing surface (LS) for two RV configurations was performed. Data on the flow structure in the region between RV and LS as dependent on the RV-to-LS distance, on the angle of RV-axis inclination to the LS plane, and on the jet flow conditions of model propulsion system were obtained. Optic shlieren visualization of the flow pattern in the region between RV and LS was performed with the help of shadow device and soot-oil visualization of limit streamline on the landing surface was made. A description of the RV models, the jet facility of ITAM SB RAS, and the automated data acquisition system is presented. On increasing the RV-to-LS distance the action of supersonic jets on RV diminishes. In the region between RV and LS, a reverse flow directed towards the RV frontal

panel forms. It is shown that the using the configuration of plumes braking system with eight nozzles located on the lateral surface of RV substantially reduces the action of reflected from landing surface supersonic jets on the RV body. Numerical simulations data were found about the flow structure in the region between RV and LS in the presence of braking jets proved to be in a satisfactorily agreement with experimental data.

References

- [1] N.A. Zheltukhin and V.I. Zapryagaev. Some characteristics of the interaction of an annular jet with a flat obstacle. In book: Gas-Dynamics and Acoustics of Jet Flows, Novosibirsk, 1979, pp. 37-60.
- [2] V.T. Kalugin and A.Yu. Lutsenko. An experimental study of the flow past entry vehicles with jet-controlled aerodynamic characteristics // Fluid Dynamics, 1996, Vol. 31, Iss. 3, pp. 434-442.

Copyright Statement

The authors confirm that they, and/or their company or organization, hold copyright on all of the original material included in this paper. The authors also confirm that they have obtained permission, from the copyright holder of any third party material included in this paper, to publish it as part of their paper. The authors confirm that they give permission, or have obtained permission from the copyright holder of this paper, for the publication and distribution of this paper as part of the ICAS 2014 proceedings or as individual off-prints from the proceedings.